# On the Stability of Advanced Power Electronic Converters: The Generalized Bode Criterion

David Lumbreras, *Student Member, IEEE*, Ernesto L. Barrios, *Member, IEEE*, Andoni Urtasun, *Member, IEEE*, Alfredo Ursúa, *Member, IEEE*, Luis Marroyo, *Member, IEEE*, and Pablo Sanchis, *Senior Member, IEEE*

***Abstract*—A key factor in the design of power electronic converters is the development of control systems and, in particular, the determination of their stability. Due to ease of application, the Bode criteria are currently the most commonly used stability criteria, with regard to both its classic version and to the subsequent revisions proposed in the literature. However, as these criteria have a limited range of applicability, on occasions, it is necessary to resort to other universally applicable criteria, such as the Nyquist criterion. Unlike Bode, the Nyquist criterion can always be applied, although its use considerably complicates the tuning of the controller. This paper proposes a new stability criterion, called generalized Bode criterion, which is, on the one hand, based on the Nyquist criterion, and therefore, always applicable, and, on the other hand, calculated from both the Bode diagram and the 0 Hz phase of the open-loop transfer function, thus, making the criterion easy to be applied. This way, the proposed criterion combines the advantages of Nyquist and Bode criteria and provides an interesting and useful tool to be applied to the controller design process. The criterion is validated by means of simulation and experimental tests made on a voltage control loop for a stand-alone photovoltaic (PV), system, including a battery, a boost converter, an inverter, and an ac load. The tests are also used to show the limitations of the classic Bode criterion and its revisions to correctly determine the stability of complex systems.**

***Index Terms*—Control systems, frequency domain analysis, Nyquist, stability, stability criteria.**

## I. Introduction

THE extensive installation of renewable-energy-based power generation systems [1] relates to a sharp drop in their price. However, the broad use of renewable energy systems and the price adjustment is leading to new challenges with regard to the design of electronic converters and, specifically, the analysis of their control loops and their stability [2]–[16].

Manuscript received July 5, 2018; revised October 16, 2018; accepted November 19, 2018. Date of publication December 4, 2018; date of current version June 10, 2019. This work was supported in part by the Spanish State Research Agency (AEI) and FEDER-UE under Grant DPI2016-80641-R and Grant DPI2016-80642-R, in part by the Public University of Navarre through a doctoral scholarship, and in part by the Ingeteam Power Technology. Recommended for publication by Associate Editor T. Suntio. *(Corresponding author: Pablo Sanchis.)*

The authors are with the Department of Electrical, Electronic and Communications Engineering and the Institute of Smart Cities, Public University of Navarre, 31006 Pamplona, Spain (e-mail:

In short, the traditional Bode criterion and its revisions still have limited applicability for power electronics, having to resort for certain systems, to design rules that are not theoretically justified and are too restrictive. In order to correctly analyze the control of these systems, other stability criteria need to be used. The Maxwell or Routh criteria are criteria that can always be applied, yet they complicate the controller tuning process as they work directly with the characteristic polynomial of the closed-loop transfer function of the system. The Nyquist criterion, which can also be applied to any system, uses information from the open-loop transfer function, but, in practice, is still difficult to apply to the controller design process as it is not intuitive [29] and it makes both the stability analysis and the controller tuning more complicated [10], [30], [31].

It is therefore clear that, in order to study the control of power electronic converters, it is necessary to have a stability criterion that can always be used and that is easy to apply to the controller design. This paper proposes a new criterion called generalized Bode criterion (GBC), which is based on the Nyquist stability criterion but is applied from the information obtained from the system open-loop Bode diagram and the 0 Hz phase. Therefore, the proposed criterion combines the advantages of the Nyquist and Bode criteria. It can be applied to any system whatsoever, being based on the Nyquist criterion, and it is also easy to apply to the design of controllers, as it uses information from the Bode diagram.

This paper is organized as follows. Section II makes a state-of-the art review of the classical stability criteria. Section III develops and formulates the proposed GBC and identifies the conditions under which the Bode criterion and its revisions are applicable. Section IV goes on to study different power electronics examples and to classify them according to the proposed criterion. Finally, in Section V, the validity of the criterion is demonstrated at a simulation level and also with experimental results in a system with an RHP pole in which the Bode criterion and its revisions cannot be applied, but where it is possible to apply the proposed criterion, which correctly determines stability.

## II. State-of-the-Art of Stability Criteria

### A. Maxwell's Criterion

Maxwell determined that, for a system to be stable, all the closed-loop transfer function poles must have a negative real part [18]. Although the advantage of this criterion is that it can be applied to any system whatsoever, it is not normally used in the design of control loops due to the fact that it is difficult to analyze how the controller parameters affect the closed-loop poles of the system.

### B. Nyquist Criterion

According to the Nyquist criterion, a system will be stable if the number of open-loop transfer function poles in the RHP $P$ is equal to the number of times that the Nyquist diagram for this function makes anti-clockwise encirclements at point $(-1, 0j)$, $N$ [20]. Although this criterion can also be applied to any system, yet again it is difficult to analyze the influence of the controller on the Nyquist diagram and, therefore, to carry out the controller design task [10], [30], [31]. This difficulty is shown in Section IV-A when the Bode and Nyquist diagrams of a studied application are compared. Moreover, on occasions, it can be a complex task to count $N$.

### C. Bode Criterion and Its Revisions

The Bode criterion determines that a system is stable if both its open-loop phase margin PM and gain margin GM are positive [21]. This is the most used criterion in power electronics systems due to the fact that the Bode diagram of the open-loop transfer function is the sum of the Bode diagrams of the non-compensated open-loop transfer function and the controller transfer function, what makes the analysis of the influence of the controller on the system response much easier. The main disadvantage of this criterion is that it can only be applied if the system satisfies certain conditions, as will be detailed later on, due to the fact that it is based on a series of specific cases of the Nyquist criterion.

Revisions have been made in order to extend the applicability of this criterion. In [24], the criterion is extended so that it can be applied to systems with more than one gain margin. This criterion, hereinafter called revised Bode criterion I, determines that a system is stable if its open-loop transfer function has no RHP poles (i.e., $P = 0$) and all its gain margins are positive [24]. Having positive gain margins mean that all the crossings of the Bode diagram with phase $\pm n{\cdot}180^\circ$ (where $n$ is an odd number) take place with gain lower than 0 dB.

In [25], another modification is proposed, hereinafter called revised Bode criterion II, which permits the application of the Bode criterion to systems whose open-loop transfer function does have poles in the RHP, determining that a system is stable if it satisfies the next condition

$$S^+ - S^- = \begin{cases} \frac{P+1}{2} & \text{for 0 and 1 integrator} \\ \frac{P}{2} & \text{for 2 integrators} \end{cases} \tag{1}$$

where $S^+$ and $S^-$ indicate the number of times that the open-loop transfer function of the Bode diagram crosses phase $\pm n \cdot 180^\circ$ (where $n$ is an odd number) with a gain greater than 0 dB and with increasing or decreasing phase, respectively, and $P$ is the number of poles in the RHP of the open-loop transfer function. The revised Bode criterion II does not analyze transfer functions with more than two integrators.

### D. Application Example

In order to understand how the previously mentioned criteria are applied, the next transfer function is analyzed

$$L(s) = 40 \cdot \frac{s+1}{s \cdot (s-0.1) \cdot (s+5)^2}. \tag{2}$$

The Bode and Nyquist diagrams of this transfer function are depicted in Fig. 1. The studied transfer function has two gain margins, namely one positive and one negative. Applying both the traditional Bode and the revised Bode criterion I, the system is determined as unstable since it has a negative gain margin.

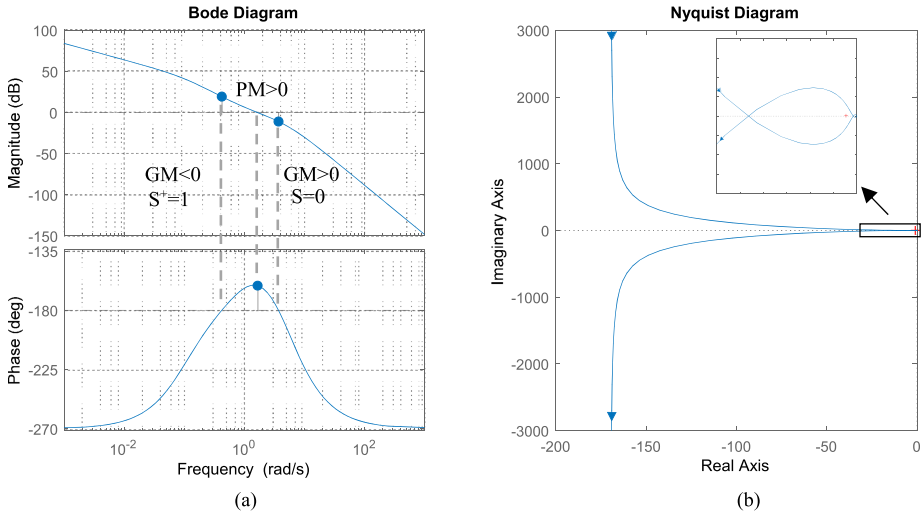


Fig. 1. Bode (left-hand side) and Nyquist (right-hand side) diagrams of transfer function in (2).

The transfer function in (2) has one RHP pole. Thus, $P = 1$. From the Bode diagram information, it can be obtained that there is a crossing with $-180°$ with increasing phase and gain higher than 0 dB (i.e., $S^+ = 1$). Another crossing with $-180°$ and decreasing phase exists, but its gain is lower than 0 dB and it is therefore not counted. By applying (1), the revised Bode criterion II determines that the system is unstable since $1 - 0 \neq 1/2$. Finally, the stability is checked with the Nyquist criterion. The number of encirclements around $(-1, 0j)$ is equal to 1. According to the Nyquist criterion, the system is stable, which demonstrates that none of the Bode criteria determines correctly the stability of the system.

## III. Proposed Stability Criterion: The GBC

### A. Development and Formulation of the GBC

The GBC proposed in this paper is based on the Nyquist criterion and is applicable to any system at all. However, it uses information from the Bode diagram, thereby considerably facilitating the design of the controller.

As it was indicated previously, to apply the Nyquist criterion, it is necessary to calculate $N$. A simple method consists in counting the crossings of the Nyquist diagram with an auxiliary half-line placed in a random direction, which starts at point $(-1, 0j)$ [32]. Thus, based on the crossings with this half-line, the Nyquist criterion can be reformulated as

$$Z = P - N = P - (N_C^+ - N_C^-) \tag{3}$$

where $N_C^+$ indicates the number of crossings between the Nyquist diagram and the half-line when the phase is increasing and $N_C^-$ indicates the number of crossings when the phase is decreasing. The positive angle is defined as the anti-clockwise rotation in relation to the real axis of the Nyquist diagram. Fig. 2 shows how it is possible to determine the number of crossings for a given half-line and, therefore, the value of $N$, which is independent of the half-line, is selected.

In [32], the proposal is to extend the concept of crossings to the Bode diagram in order to calculate $N$ using the Bode diagram instead of the Nyquist one. The relationship between

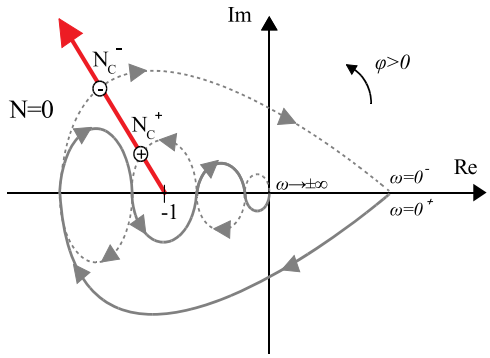


Fig. 2. Example of the Nyquist diagram, identifying the crossings with an auxiliary half-line.

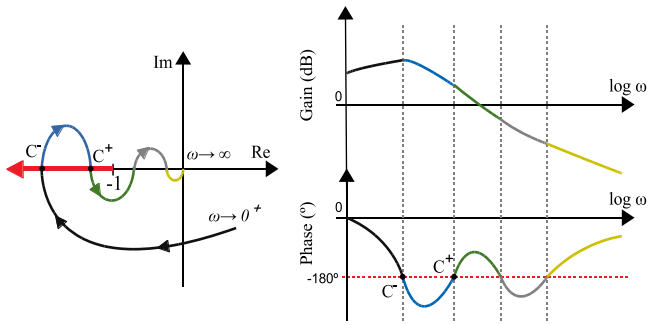


Fig. 3. Bode and Nyquist diagrams of a same system and equivalence of crossings.

diagrams means that if the half-line starting at $(-1, 0j)$ is placed in the direction of the real negative half-axis, the crossing points have a phase equal to $\pm n \cdot 180°$ (where $n$ is an odd number), and a gain greater than unity (greater than 0 dB). These points are easily identifiable on the Bode diagram, as shown in Fig. 3, where $C^+$ and $C^-$ are the crossings with the half-line counted on the Bode diagram when the phase is increasing and decreasing, respectively.

While the Nyquist diagram is defined for all frequencies, the Bode diagram is solely defined for positive frequencies. If the transfer function coefficients are real, then the Nyquist diagram

is symmetrical for positive and negative frequencies and, therefore, there are an identical number of crossings at positive and negative frequencies. This can be checked by locating the auxiliary half-line in the direction of the negative real half-axis. In the case of the diagram in Fig. 2, there would be two positive crossings $N_C^+ = 2$, one at a positive frequency $(C^+ = 1)$ and the other at a negative frequency, and two negative crossings $N_C^- = 2$, again one at a positive frequency $(C^- = 1)$ and the other at a negative frequency. The positive frequency crossings are indicated in Fig. 3.

Crossings can also occur at frequency 0 Hz called $C_0$ hereinafter, which must be counted and are key to correctly determining stability. However, these crossings are not shown on the Bode diagram, as it only includes positive frequencies.

Based on the identification between the Nyquist and Bode diagrams, and including the crossings points at 0 Hz, this paper proposes a new stability criterion called GBC, which establishes that

$$Z = P - \left[2 \cdot \left(C^+ - C^-\right) + C_0\right] \tag{4}$$

where $Z$ indicates the number of closed-loop poles in the RHP, $P$ indicates the number of open-loop poles in the RHP, $C^+$ is the number of crossings in the Bode diagram of the open-loop transfer function with phase $\pm n \cdot 180^\circ$ (with $n$ an odd number) that have gain greater than 0 dB and increasing phase, $C^-$ is the crossings counted under the same conditions as $C^+$ but with decreasing phase, and $C_0$ is the number of crossings occurring at frequency 0 Hz, taken as positive if they occur with increasing phase and as negative with decreasing phase. The calculation of $C_0$ is analyzed in Sections III-B and III-C.

From the above-mentioned equation, the necessary condition for stability can be deduced by imposing on (4) the constraint that there should be no unstable closed-loop poles (i.e., $Z = 0$). Therefore, a system will be stable if and only if

$$P = 2 \cdot \left(C^+ - C^-\right) + C_0. \tag{5}$$

In order to apply (5), the following steps are done in the open-loop transfer function. First, $P$ is obtained by inspection. Then, with the Bode diagram information, $C^+$ and $C^-$ are calculated, as shown in Fig. 3. In order to determine the system stability, only $C_0$ remains to be determined.

### *B. $C_0$ Calculation for Transfer Functions of Up To Two Integrators*

For the analysis presented ahead, the open-loop transfer function $L(s)$ is expressed in factored form as in (6), where $K_G$ is the dc gain without integrators and the number of poles is greater than the number of zeros

$$L(s) = K_G \cdot \frac{(\tau_{z,n}s+1)\ldots(\tau_{z,1}s+1)}{s^k\ (\tau_{p,m}s+1)\ldots(\tau_{p,1}s+1)} \cdot \frac{\left(\frac{1}{\omega_{z,j}^2}s^2 + \frac{2\xi_{z,j}}{\omega_{z,j}}s+1\right)\ldots\left(\frac{1}{\omega_{z,1}^2}s^2 + \frac{2\xi_{z,1}}{\omega_{z,1}}s+1\right)}{\left(\frac{1}{\omega_{p,i}^2}s^2 + \frac{2\xi_{p,i}}{\omega_{p,i}}s+1\right)\ldots\left(\frac{1}{\omega_{p,1}^2}s^2 + \frac{2\xi_{p,1}}{\omega_{p,1}}s+1\right)}. \tag{6}$$

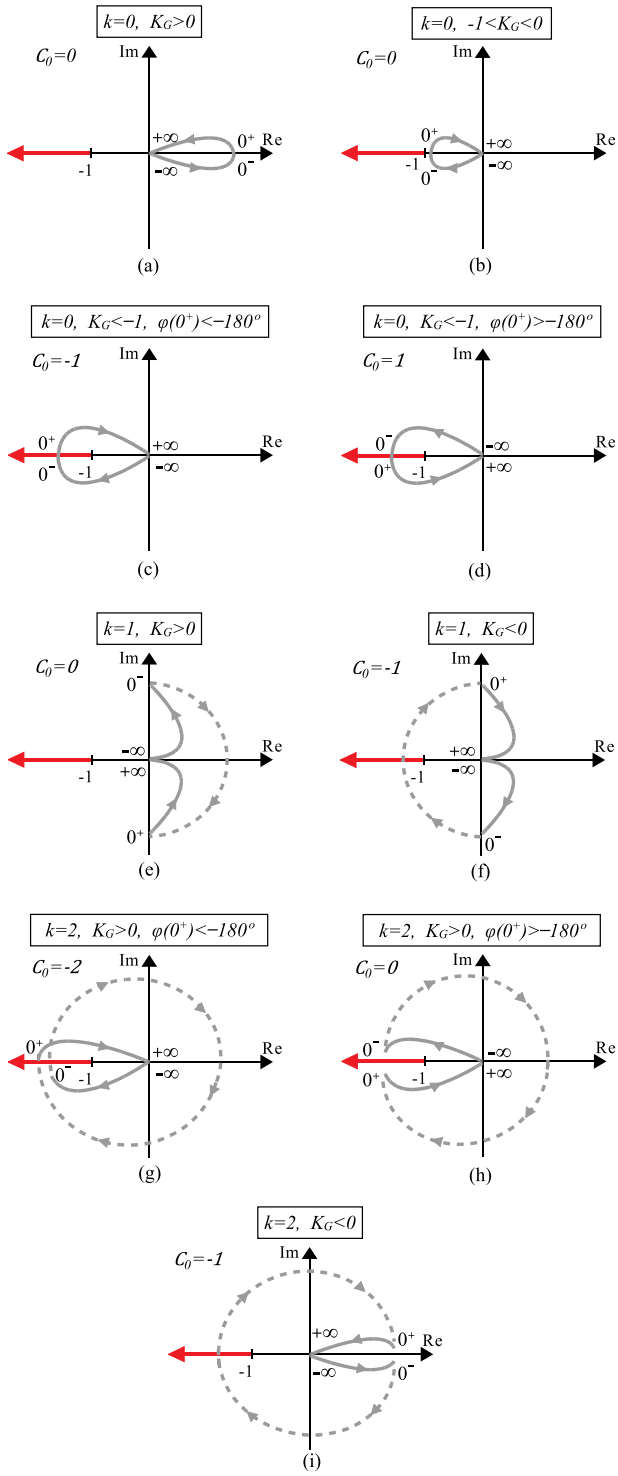


Fig. 4. Nyquist diagrams and value of $C_0$ for transfer functions of up to two integrators.

Function $L(s)$ is a generic function that has $k$ poles at origin ($k < 0$ means $-k$ zeros at origin), and $n + 2j$ zeros, and $m + 2i$ poles in the rest of the complex plane. As indicated, the function satisfies the condition $m + 2i + k > n + 2j$. For the zeros, $n$ are simple zeros, with time constants $\tau_{z,n}$, and $2j$ are complex conjugate zeros, with natural frequencies $\omega_{z,j}$ and damping factors $\xi_{z,j}$. For the poles, $m$ are simple poles, with

TABLE I
VALUE OF $C_0$ FOR OPEN-LOOP TRANSFER FUNCTIONS UP TO TWO INTEGRATORS

| Number of integrators ($k$) | dc gain without integrators ($K_G$) | Phase at $0^+$ Hz ($\varphi(0^+)$) | Crossings at zero frequency ($C_0$) |
|---|---|---|---|
| $k<0$ | - | - | 0 |
| $k=0$ | $K_G>-1$ | - | 0 |
| | $K_G<-1$ | $\varphi(0^+)<-180^o$ | –1 |
| | | $\varphi(0^+)>-180^o$ | +1 |
| $k=1$ | $K_G>0$ | - | 0 |
| | $K_G<0$ | - | –1 |
| $k=2$ | $K_G>0$ | $\varphi(0^+)<-180^o$ | –2 |
| | | $\varphi(0^+)>-180^o$ | 0 |
| | $K_G<0$ | - | –1 |

time constants $\tau_{p,m}$, and $2i$ are complex conjugate poles, with natural frequencies $\omega_{p,i}$ and damping factors $\xi_{p,i}$. Parameters $\tau$ and $\xi$ can be positive or negative, meaning that the zeros and poles can be in the LHP or RHP, respectively.

This section analyses the value of $C_0$ for transfer functions up to two integrators (i.e., $k \leq 2$), whereas the following section generalizes the calculation for any transfer function. The analyses are supported by Fig. 4, where the dashed lines indicate infinite gain. As the aim is to calculate $C_0$, particular attention is paid to what occurs between frequencies $0^-$ and $0^+$ Hz, frequencies infinitesimally smaller and greater than 0 Hz, respectively. It is important to remind that each integrator introduces a rotation in the Nyquist diagram of 180° in clockwise direction with infinite gain between $0^-$ and $0^+$ Hz [33]. Given the fact that the functions have more poles than zeros, for infinite frequencies, the Nyquist diagram is always located at the origin. The values for $C_0$ for the cases studied are summarized in Table I.

*1) No Integrators in $L(s)$ ($k = 0$):* As can be seen in Fig. 4(a)–(d), the position of the Nyquist diagram at a frequency of 0 Hz is determined by the value of $K_G$. If $K_G$ is positive, then the Nyquist diagram at 0 Hz is located on a point of the positive real half-axis [see Fig. 4 (a)]. The Nyquist diagram from frequency $0^-$ to $0^+$ Hz does not produce any crossings with the auxiliary half-line, which is painted in red in the graphics, being in this case $C_0 = 0$. If $K_G$ is negative, then the Nyquist diagram at 0 Hz is located at a point on the negative real half-axis, given that $K_G$ introduces $-180°$ at a frequency of 0 Hz. In this case, if $-1 < K_G < 0$, then the shift from $0^-$ to $0^+$ Hz on the Nyquist diagram occurs at a point with phase $-180°$ but with a gain lower than 0 dB, not leading to crossings with the half-line, so that $C_0 = 0$ [see Fig. 4(b)]. On the other hand, if $K_G < -1$, the Nyquist diagram from $0^-$ to $0^+$ Hz crosses over a point with phase $-180°$ and a gain greater than unity, producing a crossing with the half-line. Depending on whether the $0^+$ Hz phase is slightly smaller or greater than $-180°$, $C_0 = -1$ and $C_0 = 1$ is obtained, respectively, as shown in Fig. 4(c) and (d).

*2) One Integrator in $L(s)$ ($k = 1$):* In this case, the presence of the integrator gives the Nyquist diagram a clockwise rotation of 180° between $0^-$ and $0^+$ Hz with an infinite gain. The integrator also introduces $-90°$ at a frequency of 0 Hz. Two possible cases can be distinguished. If $K_G$ is positive, then it does not introduce phase, being the total phase at $0^+$ Hz $-90°$. This case gives rise to $C_0 = 0$. If $K_G$ is negative, it introduces another $-180°$ at a frequency of 0 Hz, being the total phase at $0^+$ Hz $-270°$, and obtaining a value of $C_0 = -1$. Both cases are illustrated in Fig. 4(e) and (f), respectively.

*3) Two Integrators in $L(s)$ ($k = 2$):* The two integrators cause the Nyquist diagram to rotate clockwise 360° between $0^-$ and $0^+$ Hz and with infinite gain. Furthermore, they introduce $-180°$ at a frequency of 0 Hz. Again, the total phase at 0 Hz depends on the sign of $K_G$. If $K_G$ is positive, then the total phase at 0 Hz is $-180°$, obtaining a value of $C_0$ equal to $-2$ or 0 if the phase at $0^+$ Hz is, respectively, slightly less or slightly greater than $-180°$, as shown in Fig. 4(g) and (h). If $K_G$ is negative, then the total phase at 0 Hz is 0°, being in this case $C_0 = -1$, as shown in Fig. 4(i).

*4) $L(s)$ With Zeros at the Origin ($k < 0$):* This is the simplest case, given the fact that the zeros at the origin cause the Nyquist diagram to be located at the origin of the complex plane for frequency 0 Hz. Moreover, there is no rotation with infinite gain [33]. Consequently, $C_0 = 0$.

### C. Generalization of the Calculation of $C_0$ for Any Transfer Function

As shown in the examples of Fig. 4 and Table I, the calculation of $C_0$ depends on the number of integrators, on the sign and the value of $K_G$, and, on occasions, on the exact phase at $0^+$ Hz. The calculation of $C_0$ for any transfer function is generalized ahead. In order to simplify the notation, all the phase contributions are calculated as multiples of 90°.

*1) Odd Number of Integrators in $L(s)$ ($k > 0$ and Odd):* Each integrator introduces a phase of $-90°$. Therefore, the contribution of the $k$ integrators at a frequency of 0 Hz $\theta_{\text{int}}$ can be expressed as

$$\theta_{\text{int}} = -k. \tag{7}$$

In turn, $K_G$ provides at 0 Hz a phase of 0° or $-180°$ depending on its sign. In multiples of 90°, this phase $\theta_{K_G}$ can be calculated as

$$\theta_{K_G} = \text{sign}\,(K_G) - 1 \tag{8}$$

where *sign* is a function that takes the value 1 when the sign is positive and $-1$ when it is negative.

The total phase at 0 Hz $\theta_0$ is obtained by the sum of (7) and (8). It is then necessary to normalize this phase between 0 and $-3$ (in other words, between 0 and $-270°$) through (9), where $\theta_{\text{TOT}}$ is the total normalized phase and *fix* is the function of MATLAB, which serves to round value $\theta_0/4$ to the integer value closest to zero, which is given by

$$\theta_{\text{TOT}} = 4 \cdot \left[ \frac{\theta_0}{4} - \text{fix}\left( \frac{\theta_0}{4} \right) \right]. \tag{9}$$

From here, the value of $C_0$ for these systems can be obtained by

$$C_0 = \frac{\theta_{\mathrm{TOT}} + 1}{2} - \frac{k-1}{2} \ (k \text{ odd}) \tag{10}$$

where the first term counts whether or not there has been a crossing, depending on the value of the total normalized phase, and the second term adds additional crossings due to the fact that at every two integrators, there is a 360° rotation with infinite radius.

*2) Even Number of Integrators in $L(s)$ ($k > 0$ and Even):* When $k$ is an even number, the total phase at 0 Hz is always located at 0° or −180°. In this second case, it is necessary to know whether at $0^+$ Hz, the phase is slightly greater or less than −180°.

For this purpose, the first step is to calculate the phase of the transfer function without integrators $L_0(s)$, expressed in (11). Subsequently, this expression is derived and it is evaluated for a frequency of 0 Hz. The result $\varphi_0'$ is shown in (12)

$$\begin{aligned}\varphi\ (L_0\,(j\omega)) &= \tan^{-1}(\tau_{z,n}\omega)\ + \cdots + \tan^{-1}(\tau_{z,j+1}\omega) + \\ &+ \tan^{-1}\left(\frac{2\xi_{z,j}\omega_{z,j}\omega}{\omega_{z,j}^2 - \omega^2}\right) + \cdots + \tan^{-1}\left(\frac{2\xi_{z,1}\omega_{z,1}\omega}{\omega_{z,1}^2 - \omega^2}\right) - \\ &- \tan^{-1}(\tau_{p,m}\omega) - \cdots - \tan^{-1}(\tau_{p,i+1}\omega) - \\ &- \tan^{-1}\left(\frac{2\xi_{p,i}\omega_{p,i}\omega}{\omega_{p,i}^2 - \omega^2}\right) - \cdots - \tan^{-1}\left(\frac{2\xi_{p,1}\omega_{p,1}\omega}{\omega_{p,1}^2 - \omega^2}\right)\end{aligned} \tag{11}$$

$$\begin{aligned}\varphi_0' &= \left.\frac{d\varphi\,(L_0\,(j\omega))}{d\omega}\right|_{\omega=0} \\ &= \tau_{z,n}\ + \cdots + \tau_{z,j+1} + \frac{2\xi_{z,j}}{\omega_{z,j}} + \cdots + \frac{2\xi_{z,1}}{\omega_{z,1}} \\ &- \tau_{p,m} - \cdots - \tau_{p,i+1} - \frac{2\xi_{p,i}}{\omega_{p,i}} - \cdots - \frac{2\xi_{p,1}}{\omega_{p,1}}.\end{aligned} \tag{12}$$

If the sign of $\varphi_0'$ is positive, the phase increases between $0^-$ and $0^+$ Hz, and therefore, as the phase at 0 Hz is exactly −180°, the phase at $0^+$ Hz will tend to have a value slightly greater than −180°. If the derivative is negative, then the phase decreases between $0^-$ and $0^+$ Hz, and the phase at $0^+$ Hz shall have a value slightly lower than −180°.

Based on the analysis mentioned above, the value of $C_0$ for these functions can be calculated as follows:

$$\begin{matrix} -\frac{\theta_{\mathrm{TOT}}}{2} \cdot [\mathrm{sign}\,(\varphi_0')] - \frac{\theta_{\mathrm{TOT}}+2}{2} \\ -\frac{k-2}{2} \quad (k > 0 \text{ and even}) \end{matrix}. \tag{13}$$

In this case, the first and second terms serve to count the crossings depending on the value of the total normalized phase at $0^+$ Hz. These are complementary terms, so that the first only intervenes when the phase at 0 Hz tends to −180°, influencing in this case the phase derivative sign at 0 Hz. The second term only intervenes when the phase at 0 Hz tends to 0°. Just like the case of $k$ odd number, the last term counts additional crossings due to the increase in the number of integrators.

*3) No Integrators in $L(s)$ ($k = 0$):* In this particular case, the position of the diagram at frequency 0 Hz solely depends on the value of $K_G$, and, in particular, whether this is greater than or less than −1. The position at 0 Hz $\theta_{k=0}$ can therefore be obtained by

$$\theta_{k=0} = \mathrm{sign}\,(K_G + 1) - 1. \tag{14}$$

From here, the value of $C_0$ for these systems can be calculated as

$$C_0 = -\frac{\theta_{k=0}}{2} \cdot [\mathrm{sign}\,(\varphi_0')]\ \ (k = 0)\,. \tag{15}$$

### D. Limitations on the Application of the Bode Criteria

Knowing the relationship between the Nyquist and Bode diagrams, and thanks to the proposed GBC, it is possible to identify the application conditions for the Bode criterion and its revisions.

The Bode criterion requires a positive gain margin and a positive phase margin, being the only ones in the system. This conditions result in imposing $C^+ = C^- = 0$. Using the GBC, from (5), it is easy to identify that the traditional Bode criterion is only valid for systems in which $C_0 = P$.

For its part, the revised Bode criterion I requires that $P = 0$ and that all the gain margins are negative (it allows more than one phase margin). This second condition means again that $C^+ = C^- = 0$. From (5), it is obtained that the systems in which it can be applied are those which have $C_0 = 0$. Therefore, the applicability of this criterion is limited to the systems that have $C_0 = 0$ in Table I.

Finally, the revised Bode criterion II does consider RHP poles and negative gain margins. Comparing (1) and the GBC, it can be obtained that for systems with zero and one integrators, the revised Bode criterion II can only be applied if $C_0 = 0$. For systems with two integrators, the criterion has solely been developed for cases in which $K_G > 0$, this being their application condition. The revised Bode criterion II cannot be applied to systems with more than two integrators.

## IV. Application Examples

Once the GBC has been developed, it is now applied to different case studies to show its potential for both analyzing the system stability and helping in the design of the controllers. For this purpose, two cases are analyzed first in depth and simulated. The first case represents a system without poles at the origin and the second represents a system with one pole at the origin. After that, a broad number of applications are mentioned as systems where the GBC provides a useful and valuable tool to analyze stability and design controllers. These systems represent the different cases that were shown in Table I.

### A. Case Study 1: Open-Loop Transfer Function Without Integrators

The analyzed system in this first case study is the current control of a three-phase grid-tied inverter with an *LC* filter. The system is shown in Fig. 5 and its characteristics are summarized in Table II. The grid impedance, together with the *LC* filter, creates an *LCL* filter whose behavior and transfer function are

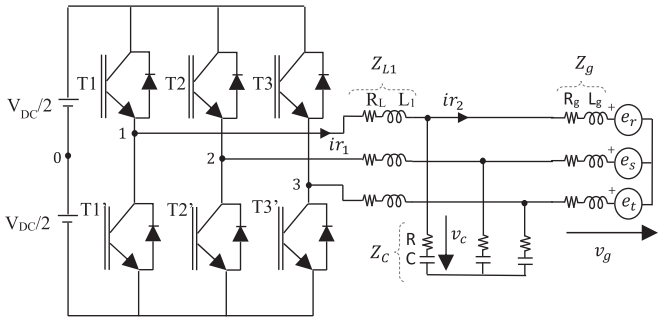


Fig. 5. Three-phase grid-tied inverter with *LC* filter.

TABLE II
CHARACTERISTICS OF THE SYSTEM IN CASE STUDY 1

| | |
|---|---|
| *Nominal power* | 100 kVA |
| *Switching frequency* | 16 kHz |
| *Current filter cut-off frequency* | 5 kHz |
| $V_{DC}$ | 800 V |
| $L_1$ | 100 μH |
| $C$ | 20 μF |
| *Grid SCR* | 12.5 |

well known [2], [8]. The inverter is connected to a 400 Vrms line voltage and 50 Hz grid.

The control scheme for the inverter current is shown in Fig. 6. It includes a proportional-resonant (PR) controller. Feedforward compensations of the dc-link voltage $v_{\rm dc}$ and the capacitor voltage $v_c$ are also included, the latter being used to both reject the grid voltage disturbance and damp the resonance [8], [9]. The delays due to computation and to zero-order-hold (ZOH) are included and modeled by the first-order Padé approximation [8]. The Bode plot of the non-compensated open-loop transfer function is shown in Fig. 7. As it can be observed, the *LCL* resonance is well damped, whereas the anti-resonance remains.

The PR controller used in this system has three resonant terms, namely one at grid frequency, to improve the reference tracking, and two more at fifth and seventh harmonic frequencies, to improve the current quality. For this system, all resonant terms are placed below the open-loop crossover frequency. Then, the PR transfer function can be expressed as follows [34]:

$$\mathrm{PR} = Kp \cdot \left(1 + \frac{K_f \cdot \omega_c \cdots}{s^2 + \omega_c \cdots + \omega_f^2} + \frac{K_5 \cdot \omega_c \cdots}{s^2 + \omega_c \cdots + \omega_5^2} + \frac{K_7 \cdot \omega_c \cdots}{s^2 + \omega_c \cdots + \omega_7^2}\right) \tag{16}$$

where $\omega_f$ is the grid frequency, $\omega_5$ and $\omega_7$ are the fifth and harmonic frequencies and $\omega_c$ is the resonant bandwidth of the resonant term, which is chosen as 5 rad/s [35], [36].

The open loop does not have RHP poles. Then, according to the GBC, the system will be stable if and only if

$$2 \cdot \left(C^+ - C^-\right) + C_0 = 0. \tag{17}$$

The open-loop transfer function does not have integrators either $(k = 0)$. Regardless of the resonant gains values, it will always have positive dc gain. Therefore, from Table I, $C_0 = 0$ and the stability condition can be reduced to

$$C^+ - C^- = 0. \tag{18}$$

Once the stability condition has been established, the controller can be designed. In first place, $K_p$ is adjusted to obtain a phase margin of 45°. The resulting open-loop crossover frequency is 800 Hz, being this frequency above the resonant terms as indicated previously. Then, according to [34], the resonant gains are designed for an open-loop gain of 50 dB. The resulting open-loop Bode diagram is illustrated in Fig. 8 together with the Nyquist diagram.

From the information provided by the Bode plot of Fig. 8, it can be concluded that the system meets the stability condition given in (18), since there are two 180° crossings with increasing phase $(C^+ = 2)$ and two more with decreasing phase $(C^- = 2)$, all of them caused by the resonant terms.

Finally, the current control is simulated in Simulink, where the PR controller is discretized with the Tustin with prewarping method, as suggested in [37]. A non-ideal grid voltage source is included in the simulation with a value of 3% of the nominal grid voltage for the fifth and seventh harmonics. Fig. 9 shows the reference and measured current. As expected, the designed PR controller achieves an accurate tracking and a satisfactory harmonic rejection. Moreover, although some negative gain margins in the Bode diagram from Fig. 8 exist, the system is stable as predicted by the easy analysis performed with the GBC.

This first case example has shown the potential of the GBC to be easily used both in the stability analysis and in the design of the controller. On the contrary, if the analysis had been made on the basis of the Nyquist diagram shown in Fig. 8, it would have been more difficult due to the complexity of this diagram. In particular, in the Nyquist diagram, it is not intuitive to know how variations either in the system or in the controller affect the stability, which is easy to investigate with the GBC. For example, in the Bode diagram of Fig. 8, it can be seen that the anti-resonance of the *LCL* filter is close to producing 180° crossings, something that is difficult to see in the Nyquist diagram. With the GBC, it is easy to see that these crossings would not be a problem in case of appearing since they would have negative gain and, therefore, would not be counted.

Finally, it is worth to mention that, since the proposed criterion is applied together with the Bode diagram, the useful information provided by this diagram, such as crossover frequencies, gain and phase margins, etc., remains available for the controller design process.

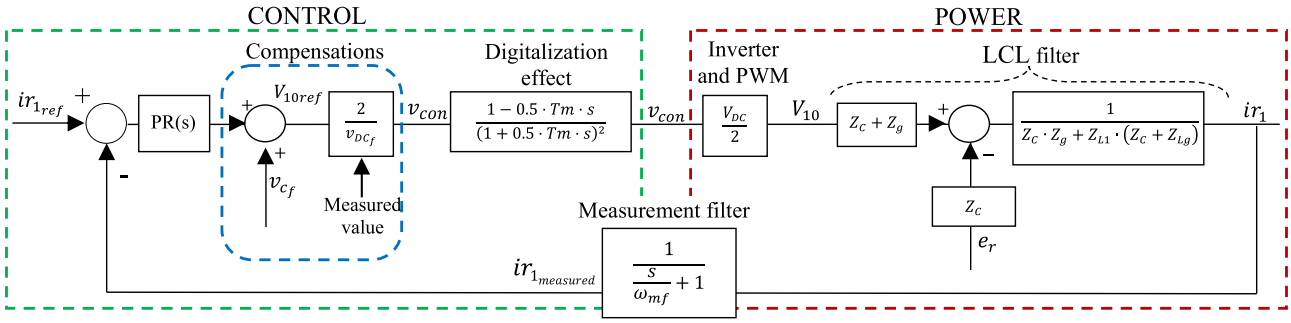


Fig. 6. Current control loop with PR controller for the case study 1.

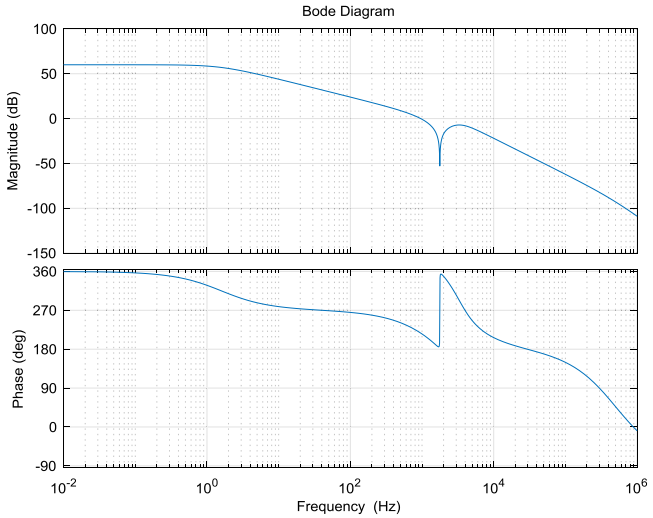


Fig. 7. Bode plot of the open loop of case study 1 without including the controller.

### B. Case Study 2: Open-Loop Transfer Function With One Integrator

The dc-link voltage control of the application shown in Fig. 10 is now selected. It consists of a battery system, a boost converter, a group of PV panels directly connected to the converter dc bus, and a single phase stand-alone inverter connected to an ac load.

This conversion system has already been studied in previous publications [22], [38], [39]. At the times in which the photovoltaic (PV) power $P_{\rm pv}$ is greater than that required by load $P_{\rm ac}$ the batteries are charged by absorbing the surplus PV power. Otherwise, the batteries deliver the remaining power and are discharged.

The boost converter is controlled by a cascade control loop, whereby the external control loop controls the bus voltage $v_{\rm dc}$ generating the reference for the internal control loop, responsible for controlling the current through the inductor $i_L$ [14], [15], [22]. The control diagram is shown in Fig. 11, where the voltage filter corresponds to the first-order approximation of the implemented moving average filter to eliminate the component at double the frequency of the ac load.

To obtain the system plant $G(s)$, a small-signal system analysis was made of the system, whereby the small-signal variables are marked with a circumflex and the steady-state values are capitalized. The dynamic resistance of panel $R_{\rm pv}$ represents the small-signal transfer function of the characteristic $I-V$ of the PV panels. The inverter and ac load are modeled as a constant power load. Operating, the $G(s)$ function is [22]

$$G\ (s) = \frac{\widehat{v_{\rm dc}\ (s)}}{\widehat{i_L\ (s)}} = \frac{V_{\rm bat}}{V_{\rm dc}} \cdot \frac{-1}{C \cdot \omega_p} \cdot \frac{-\frac{s}{\omega_z}+1}{-\frac{s}{\omega_p}+1} \tag{19}$$

where

$$\omega_z = \frac{V_{\rm bat}}{L \cdot i_L} \tag{20}$$

$$\omega_p = \frac{1}{C} \cdot \left(\frac{P_{\rm pv}}{V_{\rm dc}^2} - \frac{1}{R_{\rm pv}}\right). \tag{21}$$

Fig. 12 shows the final control diagram where the inner current control loop is approximated by a gain, as it is assumed to be much faster than the voltage control loop. Again, the digitization time delays due to computation and ZOH are modeled by the first-order Padé approximation [8]. Finally, feed-forward compensations are included with the measured and filtered bus and battery voltages.

Function $G(s)$ contains a zero in the complex RHP $\omega_z$ and a pole $\omega_p$ that can either be in the LHP or RHP. When operating at higher voltages than the one corresponding to the maximum power point (MPP), the pole is located in the LHP. As the operating voltage decreases, the pole shifts toward the RHP and enters it when the operating voltage is below the one of MPP. This is a common phenomenon due to the *P–V* characteristic of the photovoltaic panel [14], [15], [22]. The airborne wind turbine system and some motor drive applications show a similar phenomenon, with movement of a pole between the LHP and RHP depending on the direction of power flow through the system ac/dc converter [16], [23].

The value of $\omega_p$ depends on the capacitor value and the characteristics of the photovoltaic panels and its voltage operating point, which in turn depends on the irradiance and temperature. An example of the values of the pole in terms of frequency $f_p$ for different conditions of irradiance, ambient temperature, and operating voltage is shown in Fig. 13. The graphs correspond to the photovoltaic system that will be used in the experimental results, the characteristics of which are given in Table III.

The variation of the pole between the RHP and LHP must be taken into account in the controller design. At present, a rule of thumb is commonly applied in the controller design process, consisting in setting a loop crossover frequency that is double the greatest frequency at which the pole can appear in the RHP [14], [15], [22], [23], [26].

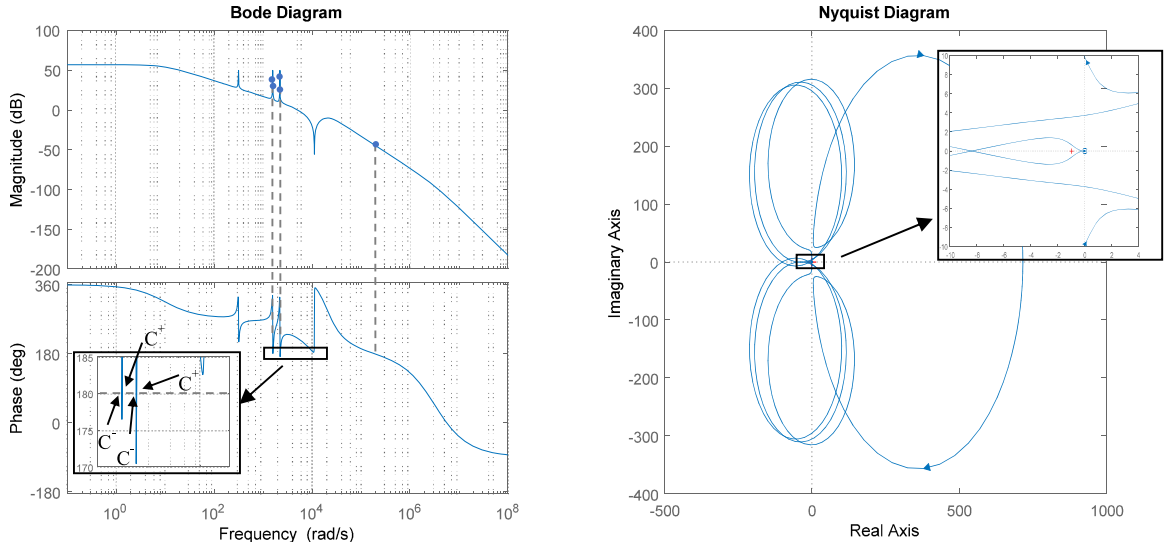


Fig. 8. Bode (left-hand side) and Nyquist (right-hand side) diagrams of the open loop in Fig. 6.

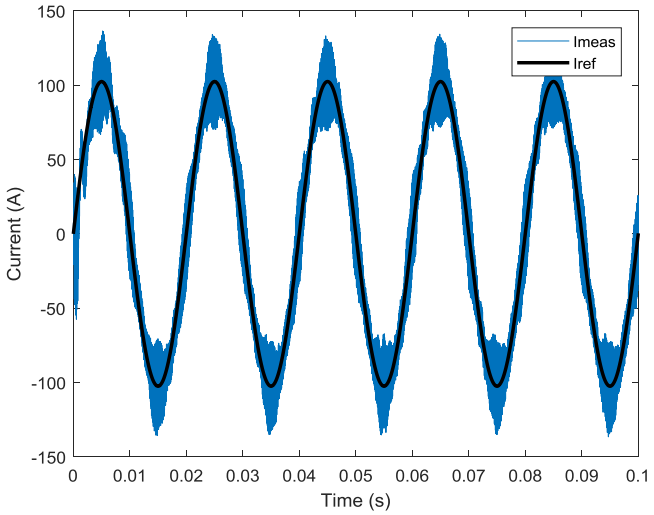


Fig. 9. Comparison of reference and measured currents with the designed PR controller.

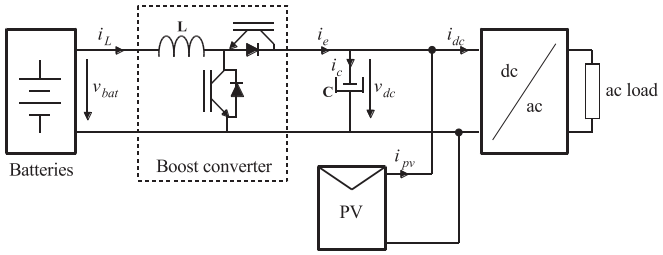


Fig. 10. Analyzed application in case study 2.

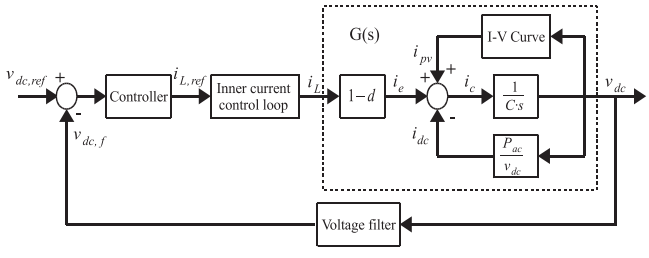


Fig. 11. Control structure for the analyzed system.

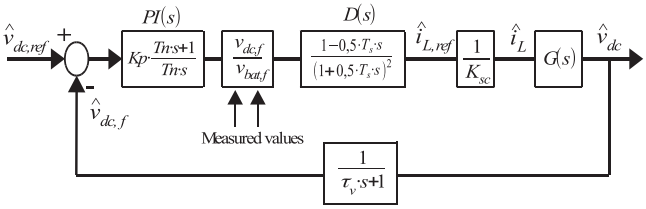


Fig. 12. Control loop of $v_{\mathrm{dc}}$.

For the case under study, the controller will be designed following this rule of thumb. It is first necessary to determine the maximum frequency at which the pole appears in the RHP.

In the studied system, the situation that would cause the system to operate at a lower voltage is considered to be a 2 kW positive load step operating close to the MPP. For the given bus capacitor value and depending on the control loop crossover frequency, this load change entails a voltage drop of between 30 and 40 V. Therefore, the minimum operating voltage for the system is set to 150 V, which for the worst irradiance and temperature conditions corresponds to a pole frequency of 7.5 Hz, as shown by the black dot in Fig. 13. The loop crossover frequency is therefore set at 15 Hz, based on the design rule of thumb.

A proportional-integral (PI) controller was selected for this application. In order to obtain an adequate overshoot in the system, it was considered sufficient to select a phase margin of 20° in the most critical operating conditions.

The open-loop transfer function $L(s)$ is the one shown in (22), which includes two first-order filters with time constants $\tau_f$ to eliminate noise in the current reference present in the

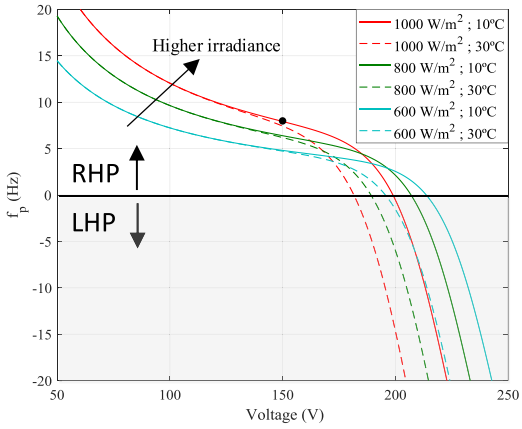


Fig. 13. Value of $f_p$ for different ambient temperature and irradiance conditions, indicating the worst operating point considered for the design.

TABLE III
CHARACTERISTICS OF THE SYSTEM IN CASE STUDY 2

| | |
|---|---|
| *PV generator peak power at STC* | 4 kWp |
| *PV generator MPP voltage and current at STC* | 216 V, 18.8 A |
| *PV generator open circuit voltage at STC* | 265 V |
| *Battery nominal voltage* | 48 V |
| *Boost converter rated power and current* | 2 kW, 60 A |
| *Boost inductance and bus capacitance* | 550 µH, 2.6 mF |

TABLE IV
CHARACTERISTICS OF THE CONTROL SCHEME

| | | |
|---|---|---|
| Sampling time | $T_s$ | 0.5 ms |
| Analog and digital filters cutoff frequency | $\tau_f$ | 0.0007957 |
| Current control loop gain | $K_{sc}$ | 10/60 V/A |
| Time constant of the voltage filter | $\tau_v$ | 5 ms |
| Switching frequency | $f_{sw}$ | 22 kHz |
| Current control loop crossover frequency | $f_{ci}$ | 2 kHz |

experimental tests subsequently conducted

$$L\ (s) = \mathrm{PI}\,(s) \cdot \frac{1}{(\tau_f \cdots + 1)^2} \cdot D\,(s) \cdot \frac{1}{K_{sc}} \cdot \frac{-1}{C \cdot \omega_p} \cdot \frac{\left(-\dfrac{s}{\omega_z} + 1\right)}{\left(-\dfrac{s}{\omega_p} + 1\right)} \cdot \frac{1}{\tau_v \cdots + 1} \quad . \quad (22)$$

The complete control scheme characteristics are provided in Table IV, which, together with the imposed design restrictions for the worst operating point, give $K_p = 0.051$ y $T_n = 0.202$. The resulting Bode diagram is shown in Fig. 14.

As it has been explained, the open-loop transfer function has one pole in the RHP. Thus, $P = 1$. In addition, as the system has one integrator and negative dc gain, from Table I, $C_0 = -1$.

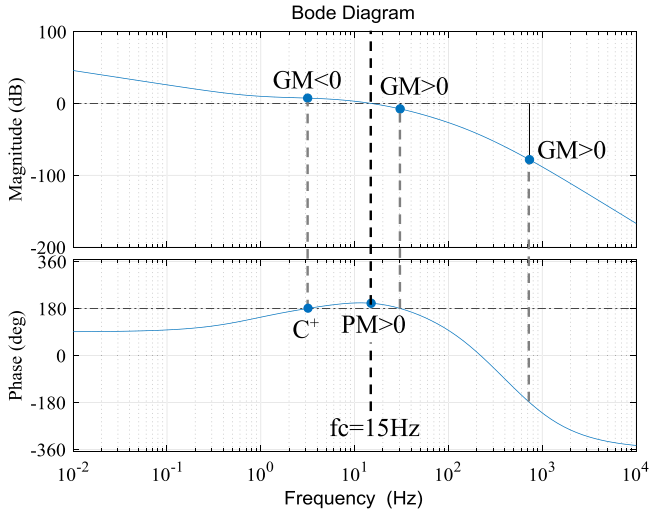


Fig. 14. Bode diagram of transfer function in (22) with the designed controller.

From Fig. 14, the number of crossings is obtained: $C^+ = 1$ and $C^- = 0$. With this information, the GBC determines that the system is stable. This information is checked against the Maxwell criterion, which also determines that the system is stable, given the fact that all the poles of the closed-loop transfer function of the system have negative real part. The simulation results concerning this case study, together with the experimental tests, that validate the analysis are shown in Section V.

### C. Other Examples of Application

Apart from the two examples studied in the previous sections, the wide variety of power electronics systems makes it possible to find examples for all the different cases of Table I. In order to validate the applicability of the GBC, this section analyses some of these examples, which are summarized in Table V.

*1) $K_G > 0$ and $k \geq 0$:* A PR controller applied to the current control of an inverter with an *L* or *LCL* filter is an example of an open-loop system with $k = 0$ and $K_G > 0$, which leads to $C_0 = 0$, as shown in Table V. This has been the example of case study 1, but this is also the case for systems whose behavior can be modeled by a first-order transfer function (e.g., induction motors) and are controlled with PR controllers. However, if a PI or a proportional-integral-resonant controller is used in these applications [13], [34], [36], [40], an open loop with one integrator and positive gain is obtained (i.e., $k = 1, K_G > 0$), corresponding to another case of Table V, which also has $C_0 = 0$.

The use of a double PI controller (named PII controller from now on) can improve the disturbance rejection and, therefore, the reference tracking [41], [42]. If again, the inverter from case study 1 or similar systems is controlled with a PII controller, an open loop with two integrators and positive gain is obtained (i.e., $k = 2, K_G > 0$). As it has been shown in (12) (see Section III-C) and Table V, depending on the zeros and poles of the transfer function, two different cases, with $C_0 = 0$ or $C_0 = -2$, can occur.

Another application with positive gain and two integrators in the open-loop transfer function is the synchronous reference

TABLE V
EXAMPLES OF APPLICATION FOR THE DIFFERENT CASES OF TABLE I

| $k$ | $K_G$ | Phase at $0^+$ Hz ($\varphi(0^+)$) or sign of the phase derivative at 0 Hz ($\varphi'_0$) | $C_0$ | Examples |
|---|---|---|---|---|
| $k<0$ | - | - | 0 | Active damping: using the capacitor current through a proportional gain [50]-[53] or the capacitor voltage through a derivative [50], [51], [54] |
| $k=0$ | $K_G>-1$ | - | 0 | Case study 1 (grid-tied inverter or system modelled by a first order transfer function) with a PR controller (section IV.A) |
| | $K_G<-1$ | $\varphi(0^+)<-180^o$ or $\varphi'_0<0$ | −1 | Case study 2 (dc-link voltage control loop from the system in [22], [38], [39]) with a proportional controller |
| | | $\varphi(0^+)>-180^o$ or $\varphi'_0>0$ | +1 | |
| $k=1$ | $K_G>0$ | - | 0 | Case study 1 (grid-tied inverter or system modelled by a first order transfer function) with a PI or a PIR controller [13], [34], [36], [40] |
| | $K_G<0$ | - | −1 | Case study 2 (dc-link voltage control loop from the system in [22], [38], [39]) with a PI controller (section IV.B) |
| $k=2$ | $K_G>0$ | $\varphi(0^+)<-180^o$ or $\varphi'_0<0$ | −2 | Case study 1 (grid-tied inverter or system modelled by a first order transfer function) with a PII controller<br>Synchronous reference frame phased-locked loop (PLL) [43]-[46]<br>Inverter dc-link voltage control with PI controller [47]-[49] |
| | | $\varphi(0^+)>-180^o$ or $\varphi'_0>0$ | 0 | |
| | $K_G<0$ | - | −1 | Case study 2 (dc-link voltage control loop from the system in [22], [38], [39]) with a PII controller |

frame phased-locked loop (PLL) [43]–[46], in which the first integrator comes from a PI controller and the second one is due to the integration needed to transform the frequency into the angle position.

The dc-link voltage control of inverters in which the relationship between the capacitor voltage and current is approximated by 1/(C·s) and which includes a PI controller [47]–[49] is another example of an open loop with two integrators. The plant of these dc voltage control loops has negative gain, since it is necessary to decrease the controlled current in order to increase the dc voltage. However, it is a common practice to calculate the voltage error as the measured minus the reference voltage [47]–[49], which has the same effect as multiplying the open-loop gain by –1, obtaining positive dc gain for the open-loop transfer function, and therefore, being the same case (i.e., $k = 2, K_G > 0$) as the previous PII controller systems and PLL control loops. In these last two power electronics examples (i.e., the PLL and the dc voltage control loops), as the PI controller zero is much closer to the origin than the rest of poles and zeros in the open loop, from (12), $\varphi'_0$ is always positive, which means that the phase at 0 Hz is increasing, and therefore, $C_0 = 0$.

*2) $K_G < 0$ and $k \geq 0$:* The system analyzed in Section IV-B consisting in the voltage control of the dc-link with the PV generator (see Fig. 10) can have different controllers, all of them resulting in open-loop transfer functions with $K_G < 0$.

If a proportional controller is used, the open loop has zero integrators ($k = 0$ and $K_G < 0$). In this system, the controller gain should be high enough to obtain $K_G < -1$, and therefore, according to Table V, $C_0$ will be 1 or –1 depending on the zeros and poles of the open-loop transfer function. This case is an example of applications in which the steady-state error caused by avoiding the integral term is small or even negligible. By contrast, if a PI controller is used, the control loop is the one studied in case study 2, which means that it has $k = 1, K_G < 0$, and $C_0 = -1$. Finally, if the system is controlled with a PII controller, the open loop has two integrators and negative gain, which corresponds to $k = 2, K_G < 0$, and therefore, $C_0 = -1$.

*3) $k < 0$:* Finally, there are also power electronics examples with more zeros than poles at the origin, such as the active damping control loops of *LCL* filters. Two main different active damping implementations are usually proposed, which damp the system by using the capacitor current through a proportional gain [50]–[53] or the capacitor voltage through a derivative [50], [51], [54]. Due to the relationship between voltage and current capacitor in the first case and to the implementation of a derivative in the second case, a zero at the origin appears in the active damping open loop of both systems. They are, therefore, examples of $k < 0$ and consequently $C_0 = 0$, independently of the value of $K_G$, as shown in Table V.

*4) On the Sign of $K_G$:* Even though the proposed stability criterion can be applied to any system whatsoever, it can be noticed that the practical examples given in Table V with negative dc gain (i.e., $K_G < 0$) occur when one RHP pole appears in the open loop, whereas the examples with positive dc gain (i.e., $K_G > 0$) take place when no RHP poles exist. The reason why the two other combinations, namely $K_G < 0$ without RHP poles and $K_G > 0$ with one RHP pole, do not appear in the practical open-loop transfer functions is now explained.

By reordering (5), the proposed stability criterion can be represented by

$$C^+ - C^- = \frac{P - C_0}{2} . \tag{23}$$

As the difference between crossings is always an integer, for the system to be stable, if $P$ is an odd number, $C_0$ must be an odd number as well, which can only occur for $K_G < 0$ (see Table V). In the same way, if $P$ is zero or an even number, $C_0$ must be zero or an even number too, which can only occur for $K_G > 0$. If these conditions are not met, it is impossible to make

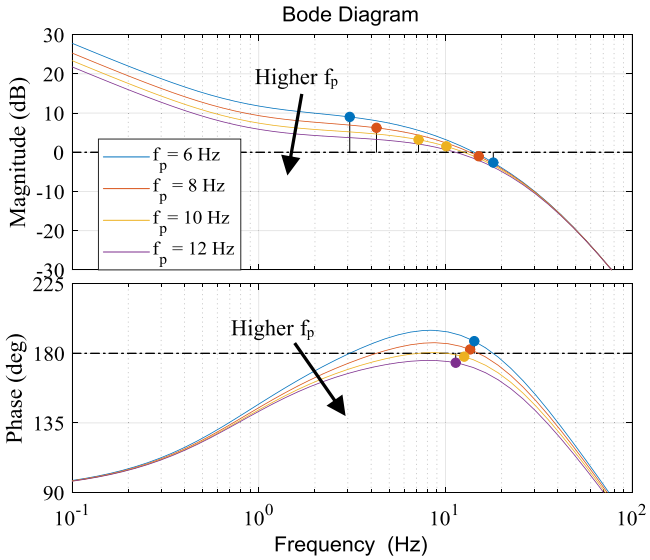


Fig. 15. Bode diagram of transfer function in (22) with the designed controller for different $f_p$ values.

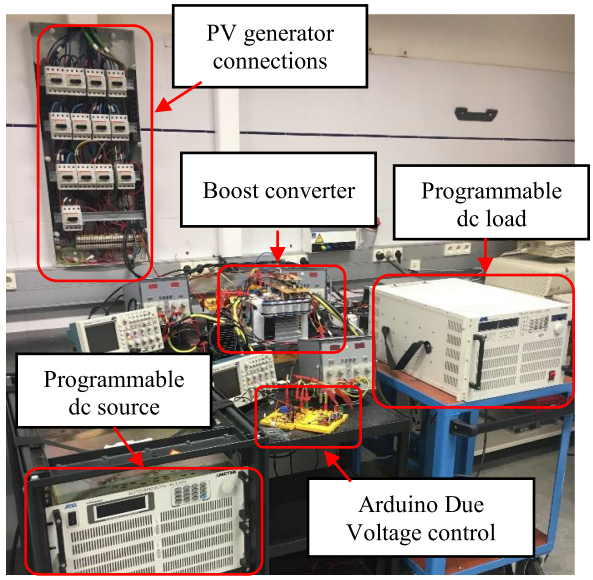


Fig. 16. Setup for the experimental tests.

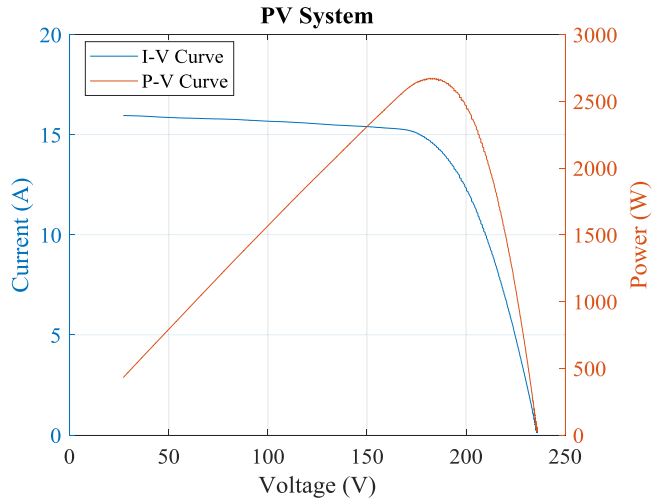


Fig. 17. Experimental *I–V* curves (blue) and *P–V* (orange) during the tests.

the system stable. In order to overcome this problem, the control designers usually multiply the open loop by –1 to change the sign of $K_G$, as it has been previously mentioned in the examples about the dc-link voltage control of inverters [47]–[49].

## V. Simulation and Experimental Results for Case Study 2

This section proposes two tests to demonstrate the GBC and to validate its application for the system of Section IV-B. Both tests are designed so that the voltage operating point changes, therefore changing the characteristics of the system until instability is reached. In order to do it, the stability limit of the system must be identified first.

The evaluation of the stability can be made with the classical stability criteria. Bode criterion should not be used to determine the stability of this system as it has more than one gain margin. In fact, if it is applied, it will determine that the system is unstable as there is a negative gain margin, as can be seen in Fig. 14. It is also not possible to apply the revised Bode criterion I, since the system also has an RHP pole. If applied, it would lead to the same wrong stability conclusion. It is not possible to apply the revised Bode criterion II either, because the system has negative dc gain and a value of $C_0 = -1$. If (1) is applied, the revised Bode criterion II would determine that the open loop is unstable as a pole lies in the RHP $P = 1$ and from the Bode diagram in Fig. 14, $S^+ = 1$ and $S^- = 0$. By contrast, the GBC proposed in this paper can be applied, and as explained previously, it determines correctly that the system is stable.

From the GBC and the Bode diagram, more information can be obtained about the system stability, being possible to evaluate the theoretical justification of the rule of thumb used in the design. In the studied system, for the worst operating point, a pole lies in the RHP and, if $K_p$ stays positive, $C_0 = -1$. From (5), it can be determined that for the studied system to be stable $2(C^+ - C^-) = P - C_0 = 1 - (-1)$. That means that the difference between positive and negative crossovers must be 1, i.e., $C^+ - C^- = 1$. This is the justification of the design rule of thumb, which thereby tries to guarantee the occurrence of a positive crossing by choosing a crossover frequency in which the RHP pole has already introduced almost all its positive phase. This condition is also the stability limit of the system, and can be used to identify the operating point after which the system becomes unstable. Fig. 15 shows the area of interest of different Bode diagrams of $L(s)$ for different $f_p$ values in the RHP (some of them even more restrictive than the design limit). As can be seen, there is a frequency slightly lower than 10 Hz, after which $C^+ - C^- \neq 1$, making the system unstable. Depending on the temperature and irradiance conditions, this pole frequency will be associated with a certain operating voltage.

Two tests are carried out first with the PSIM simulation software and then experimentally. They include the characteristics of the system shown in Table III and the control loop parameters

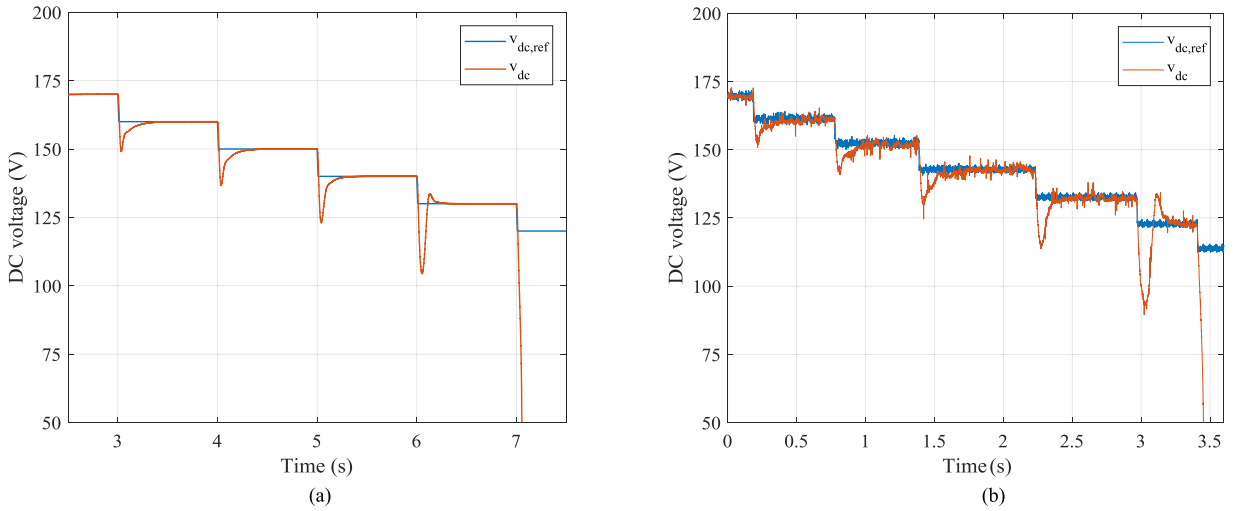


Fig. 18. Results for Test 1. (a) Simulation. (b) Experimental.

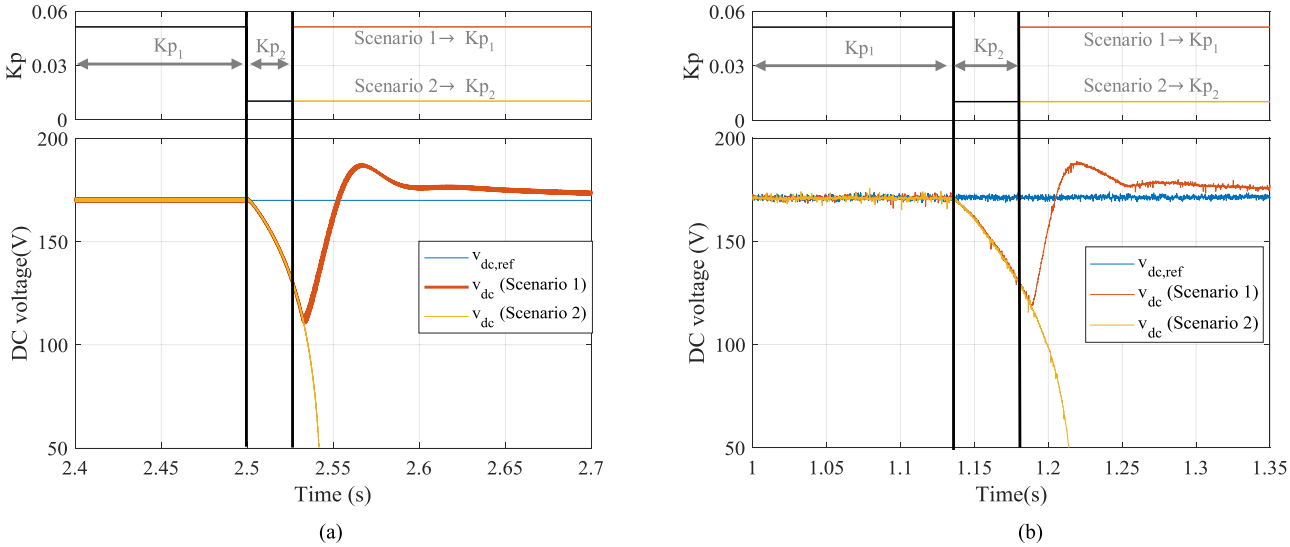


Fig. 19. Results for Test 2. (a) Simulation. (b) Experimental.

from Table IV. In each test, if the bus voltage decreases under 50 V, the system is disconnected because it reaches the nominal voltage of the batteries.

The experimental setup, shown in Fig. 16, used AMREL SPS400X75, a programmable dc power supply, instead of the batteries, a boost converter, developed at the Public University of Navarra (UPNA) with analog current control, a PV system, also located at the UPNA facilities, comprising a total of forty eight BP 585 modules, whose characteristics are shown in Table III and an AMREL PLA7.5K-600-400 programmable load, whose power output was controlled in order to physically emulate the operation of the ac load, and the inverter. At the frequencies of interest of the dc voltage control loop, the programmable load has the same effect as the inverter and ac load from Fig. 10, since both acts as constant power loads. The voltage control was implemented in an Arduino Due board.

The experimental tests were carried out on a sunny day, with a low temperature (10 °C) and clear sky, in order to have a high, practically constant irradiance value, estimated at 800 W/m$^2$. The *I–V* and *P–V* curves of the PV generator during the tests were obtained experimentally and are shown in Fig. 17. These same conditions are used for the simulation results.

### A. *Test I: Change in the PV Panel Operating Point*

This test starts in an operating point slightly below to MPP, where the load power is greater than that of the photovoltaic panels and, therefore, the batteries provide the remaining power. Starting from this voltage, steps are introduced in which the reference voltage is reduced by 10 V at a time. This test represents a progressive increase of the pole frequency, given the fact that, maintaining irradiance and temperature constant, a reduction in the operating voltage is equivalent to increase the pole frequency, as shown in Fig. 13.

The simulation results are shown in Fig. 18(a). As the voltage decreases, the system responds with greater overshoot,

oscillating at the 140 to 130 V step. Faced with a step in which the reference voltage changes from 130 to 120 V, the voltage drops and the system becomes unstable, reaching 50 V and being disconnected. The threshold voltage from which the system becomes unstable is approximately 90 V, given the fact that this is the point at which the voltage drop trend changes. For the irradiance and temperature conditions, the value of this threshold voltage is close to a pole frequency of approximately 10 Hz, as shown in Fig. 13, which is the limit that guarantees $C^+ - C^- = 1$ and, therefore, a stable system. The result is in line with the theoretically anticipated result.

The experimental results are shown in Fig. 18(b) and demonstrate that, effectively, the system becomes less stable as the operating voltage decreases, progressively increasing the overshoot (which is a bit higher than in the simulation results). Yet again, in the last voltage step, the voltage decreases under the threshold voltage, leading to system instability. In this case, the voltage at which the system becomes unstable corresponds to a voltage slightly below 90 V, which is also close to the theoretical and simulation results.

### B. Test 2: Change in the Controller Gain

This test studies two different scenarios, which again start from an operating point to the left of the MPP. At a certain instant, the original value of $K_p, K_{p1}$ is changed to a new value $K_{p2} = 0.2 \cdot K_{p1}$. This change reduces the system crossover frequency resulting in $C^+ - C^- \neq 1$, and obtaining, therefore, an unstable system. Based on this situation, in Scenario 1, the value of $K_{p1}$ is recovered when the voltage decreases under 130 V, returning to a stable system. In Scenario 2, $K_{p2}$ is maintained during the rest of the simulation.

The simulation results are shown in Fig. 19(a). These results show how, for Scenario 1, the system becomes unstable when $K_p = K_{p2}$, but it is able to recover the reference voltage when $K_p = K_{p1}$ is recovered. For Scenario 2, the system becomes unstable and the voltage decreases to 50 V when it is disconnected.

The experimental results of Fig. 19(b) also demonstrate the results previously anticipated by simulation. In Scenario 1, after recovering the original value of $K_p$, the system manages to recover the reference voltage, whereas in Scenario 2, the voltage drops to 50 V as the system becomes unstable and it is disconnected.

The simulation and experimental results show the stability limit condition, validating the GBC and demonstrating the limitation of the applicability range of the traditional Bode, revised Bode I, and revised Bode II criteria, and the risk of offering incorrect conclusions with regard to the stability of certain systems.

## VI. Conclusion

This paper proposes a new stability criterion, named GBC, which responds to the need for a stability criterion that is applicable under any conditions, being based on the Nyquist criterion, and that is easy to apply to the design of controllers, as it solely uses information from the open-loop transfer function of the Bode diagram. The proposed criterion thus combines the advantages of the Nyquist criterion applicability and Bode criteria practicability.

For the formulation of the criterion, particular attention is paid to what occurs at frequency 0 Hz, as this is one of the key stability factors. Besides, the paper also identifies and shows the limited applicability of the Bode criterion and its revisions to determine the stability of certain complex system, which could lead to incorrect conclusions with regard to stability. After that, in order to generalize the study to any transfer function, it is analyzed how the proposed criterion can be applied to the most common cases appearing in power electronics converters.

The theoretical development was validated at a simulation and experimental level, applying the criterion first to the control of the current of a three-phase grid-tied inverter with a multi-resonant controller and then to the voltage control for a stand-alone battery PV system. Two tests are carried out on the latter system, one test modifies the panel operating point until instability is achieved, whereas the other test modifies the controller. The results of the tests validate the GBC and show how this criterion helps to establish some guidelines for the controller design process.

## References


[1] Ren21, Paris, France, "Global status report," vol. 19, 2016. [Online]. Available: http//www. ren21.net

[2] W. Yao, Y. Yang, X. Zhang, F. Blaabjerg, and P. C. Loh, "Design and analysis of robust active damping for LCL filters using digital notch filters," *IEEE Trans. Power Electron.*, vol. 32, no. 3, pp. 2360–2375, Mar. 2017.

[3] M. Lu, A. Al-Durra, S. M. Muyeen, S. Leng, P. C. Loh, and F. Blaabjerg, "Benchmarking of stability and robustness against grid impedance variation for LCL-filtered grid-interfacing inverters," *IEEE Trans. Power Electron.*, vol. 33, no. 10, pp. 9033–9046, Oct. 2018.

[4] R. Pena-Alzola *et al.*, "Robust active damping in LCL-filter based medium-voltage parallel grid-inverters for wind turbines," *IEEE Trans. Power Electron.*, vol. 33, no. 12, pp. 10846–10857, Dec. 2018.

[5] V. Blasko and V. Kaura, "A novel control to actively damp resonance in input LC filter of a three-phase voltage source converter," *IEEE Trans. Ind. Appl.*, vol. 33, no. 2, pp. 542–550, Mar.–Apr. 1997.

[6] J. Dannehl, M. Liserre, and F. W. Fuchs, "Filter-based active damping of voltage source converters with LCL filter," *IEEE Trans. Ind. Electron.*, vol. 58, no. 8, pp. 3623–3633, Aug. 2011.

[7] N. He *et al.*, "Weighted average current control in a three-phase grid inverter with an LCL filter," *IEEE Trans. Power Electron.*, vol. 28, no. 6, pp. 2785–2797, Jun. 2013.

[8] J. L. Agorreta, M. Borrega, J. López, and L. Marroyo, "Modeling and control of N-paralleled grid-connected inverters with LCL filter coupled due to grid impedance in PV plants," *IEEE Trans. Power Electron.*, vol. 26, no. 3, pp. 770–785, Mar. 2011.

[9] D. Pérez-Estévez, J. Doval-Gandoy, A. G. Yepes, Ó. López, and F. Baneira, "Enhanced resonant current controller for grid-connected converters with LCL filter," *IEEE Trans. Power Electron.*, vol. 33, no. 5, pp. 3765–3778, May 2018.

[10] A. G. Yepes, F. D. Freijedo, Ó. López, and J. Doval-Gandoy, "Analysis and design of resonant current controllers for voltage-source converters by means of Nyquist diagrams and sensitivity function," *IEEE Trans. Ind. Electron.*, vol. 58, no. 11, pp. 5231–5250, Nov. 2011.

[11] D. G. Holmes, T. A. Lipo, B. P. McGrath, and W. Y. Kong, "Optimized design of stationary frame three phase AC current regulators," *IEEE Trans. Power Electron.*, vol. 24, no. 11, pp. 2417–2426, Nov. 2009.

[12] C. Liu, F. Blaabjerg, W. Chen, and D. Xu, "Stator current harmonic control with resonant controller for doubly fed induction generator," *IEEE Trans. Power Electron.*, vol. 27, no. 7, pp. 3207–3220, Jul. 2012.

[13] M. Liserre, R. Teodorescu, and F. Blaabjerg, "Multiple harmonics control for three-phase grid converter systems with the use of PI-RES current controller in a rotating frame," *IEEE Trans. Power Electron.*, vol. 21, no. 3, pp. 836–841, May 2006.

[14] T. Messo, J. Jokipii, J. Puukko, and T. Suntio, "Determining the value of DC-link capacitance to ensure stable operation of a three-phase photovoltaic inverter," *IEEE Trans. Power Electron.*, vol. 29, no. 2, pp. 665–673, Feb. 2014.

[15] J. Puukko, L. Nousiainen, and T. Suntio, "Effect of minimizing input capacitance in VSI-based renewable energy source converters," in *Proc. IEEE 33rd Int. Telecommun. Energy Conf.*, 2011, pp. 1–9.

[16] J. R. Espinoza, G. Joos, M. Perez, and T. L. A. Moran, "Stability issues in three-phase PWM current/voltage source rectifiers in the regeneration mode," in *Proc. IEEE Int. Symp. Ind. Electron.*, 2000, vol. 2, pp. 453–458.

[17] C. G. Kang, "Origin of stability analysis: 'On governors' by J.C. Maxwell [historical perspectives]," *IEEE Control Syst. Mag.*, vol. 36, no. 5, pp. 77–88, Oct. 2016.

[18] J. C. Maxwell, "I. On governors," *Proc. Roy. Soc. London*, vol. 16, pp. 270–283, 1868.

[19] E. J. Routh, *A Treatise on the Stability of a Given State of Motion: Particularly Steady Motion*. New York, NY, USA: Macmillan and Company, 1877.

[20] H. Nyquist, "Regeneration theory," *Bell Labs Tech. J.*, vol. 11, no. 1, pp. 126–147, 1932.

[21] H. W. Bode, "Relations between attenuation and phase in feedback amplifier design," *Bell Labs Tech. J.*, vol. 19, no. 3, pp. 421–454, 1940.

[22] A. Urtasun, P. Sanchis, and L. Marroyo, "Control strategy for an integrated photovoltaic-battery system," in *Proc. 19th Eur. Conf. Power Electron. Appl.*, 2017, pp. P.1–P.10.

[23] J. W. Kolar *et al.*, "Conceptualization and multiobjective optimization of the electric system of an airborne wind turbine," *IEEE J. Emerg. Sel. Top. Power Electron.*, vol. 1, no. 2, pp. 73–103, Jun. 2013.

[24] J. Hahn, T. Edison, and T. F. Edgar, "A note on stability analysis using bode plots," *Chem. Eng. Educ.*, vol. 35, no. 3, pp. 208–211, 2001.

[25] H. Unbehauen, *Regelungstechnik I: Klassische Verfahren zur Analyse und Synthese linearer kontinuierlicher Regelsysteme, Fuzzy-Regelsysteme*. Berlin, Germany: Springer, 1992.

[26] S. Skogestad and I. Postlethwaite, *Multivariable Feedback Control: Analysis and Design*, vol. 2. New York, NY, USA: Wiley, 2007.

[27] R. B. Ridley, *Power Supply Design: Control*. Bradenton, FL, USA: Ridley Engineering, Incorporated, 2011.

[28] D. Lumbreras, E. L. Barrios, A. Ursúa, L. Marroyo, and P. Sanchis, "On the stability criteria for inverter current control loops with LCL output filters and varying grid impedance," in *Proc. 19th Eur. Conf. Power Electron. Appl.*, 2017, pp. 1–10.

[29] Y. Liao and X. Wang, "General rules of using bode plots for impedance-based stability analysis," in *Proc. IEEE 19th Workshop Control Model. Power Electron.*, 2018, pp. 1–6.

[30] J. Yin, S. Duan, and B. Liu, "Stability analysis of grid-connected inverter with LCL filter adopting a digital single-loop controller with inherent damping characteristic," *IEEE Trans. Ind. Inform.*, vol. 9, no. 2, pp. 1104–1112, May 2013.

[31] K. Nakamura, K. Yubai, D. Yashiro, and S. Komada, "Controller design method achieving maximization of control bandwidth by using Nyquist diagram," in *Proc. Int. Autom. Control Conf.*, 2016, pp. 35–40.

[32] M. Vidyasagar, D. G. Meyer, and G. F. Franklin, "Some simplifications of the graphical Nyquist criterion," *IEEE Trans. Autom. Control*, vol. 33, no. 3, pp. 301–305, Mar. 1988.

[33] R. C. Dorf and R. H. Bishop, *Modern Control Systems*. London, U.K.: Pearson, 2011.

[34] D. Lumbreras, T. Schobre, and R. Mallwitz, "Systematic and easy-to-use design procedure for proportional-integral- resonant controllers keywords," in *Proc. 20th Eur. Conf. Power Electron. Appl.*, 2018, pp. 1–10.

[35] P. C. Tan, P. C. Loh, and D. G. Holmes, "High-performance harmonic extraction algorithm for a 25 kV traction power quality conditioner," *IEE Proc.—Elect. Power Appl.*, vol. 151, no. 5, pp. 505–512, 2004.

[36] Q. Yan, X. Wu, X. Yuan, Y. Geng, and Q. Zhang, "Minimization of the DC component in transformerless three-phase grid-connected photovoltaic inverters," *IEEE Trans. Power Electron.*, vol. 30, no. 7, pp. 3984–3997, Jul. 2015.

[37] A. G. Yepes, F. D. Freijedo, J. Doval-Gandoy, O. López, J. Malvar, and P. Fernandez-Comesana, "Effects of discretization methods on the performance of resonant controllers," *IEEE Trans. Power Electron.*, vol. 25, no. 7, pp. 1692–1712, Jul. 2010.

[38] R. Gules, J. D. P. Pacheco, H. L. Hey, and J. Imhoff, "A maximum power point tracking system with parallel connection for PV stand-alone applications," *IEEE Trans. Ind. Electron.*, vol. 55, no. 7, pp. 2674–2683, Jul. 2008.

[39] D. V. de la Fuente, C. L. T. Rodríguez, G. Garcerá, E. Figueres, and R. O. Gonzalez, "Photovoltaic power system with battery backup with grid-connection and islanded operation capabilities," *IEEE Trans. Ind. Electron.*, vol. 60, no. 4, pp. 1571–1581, Apr. 2013.

[40] D. G. Holmes, B. P. McGrath, and S. G. Parker, "Current regulation strategies for vector-controlled induction motor drives," *IEEE Trans. Ind. Electron.*, vol. 59, no. 10, pp. 3680–3689, Oct. 2012.

[41] U. Anwar, R. Erickson, D. Maksimović, and K. K. Afridi, "A control architecture for low current distortion in bridgeless boost power factor correction rectifiers," in *Proc. IEEE Appl. Power Electron. Conf. Expo.*, 2017, pp. 82–87.

[42] L. Cao, K. H. Loo, and Y. M. Lai, "Output-impedance shaping of bidirectional DAB DC-DC converter using double-proportional-integral feedback for near-ripple-free DC bus voltage regulation in renewable energy systems," *IEEE Trans. Power Electron.*, vol. 31, no. 3, pp. 2187–2199, Mar. 2016.

[43] S. Golestan, F. D. Freijedo, A. Vidal, A. G. Yepes, J. M. Guerrero, and J. Doval-Gandoy, "An efficient implementation of generalized delayed signal cancellation PLL," *IEEE Trans. Power Electron.*, vol. 31, no. 2, pp. 1085–1094, Feb. 2016.

[44] B. Liu, F. Zhuo, Y. Zhu, H. Yi, and F. Wang, "A three-phase PLL algorithm based on signal reforming under distorted grid conditions," *IEEE Trans. Power Electron.*, vol. 30, no. 9, pp. 5272–5283, Sep. 2015.

[45] S. Golestan, J. M. Guerrero, and J. C. Vasquez, "Three-phase PLLs: A review of recent advances," *IEEE Trans. Power Electron.*, vol. 32, no. 3, pp. 1894–1907, Mar. 2017.

[46] D. Arricibita, L. Marroyo, and E. L. Barrios, "Simple and robust PLL algorithm for accurate phase tracking under grid disturbances," in *Proc. IEEE 18th Workshop Control Model. Power Electron.*, 2017, pp. 1–6.

[47] S. M. Tayebi and I. Batarseh, "Mitigation of current distortion in a three-phase microinverter with phase skipping using a synchronous sampling DC-link voltage control," *IEEE Trans. Ind. Electron.*, vol. 65, no. 5, pp. 3910–3920, May 2018.

[48] A. Urtasun, P. Sanchis, and L. Marroyo, "Adaptive voltage control of the DC/DC boost stage in PV converters with small input capacitor," *IEEE Trans. Power Electron.*, vol. 28, no. 11, pp. 5038–5048, Nov. 2013.

[49] N. E. Zakzouk, A. K. Abdelsalam, A. A. Helal, and B. W. Williams, "PV single-phase grid-connected converter: DC-link voltage sensorless prospective," *IEEE J. Emerg. Sel. Top. Power Electron.*, vol. 5, no. 1, pp. 526–546, Mar. 2017.

[50] R. Pena-Alzola, M. Liserre, F. Blaabjerg, R. Sebastián, J. Dannehl, and F. W. Fuchs, "Systematic design of the lead-lag network method for active damping in LCL-filter based three phase converters," *IEEE Trans. Ind. Inform.*, vol. 10, no. 1, pp. 43–52, Feb. 2014.

[51] Z. Xin, P. C. Loh, X. Wang, F. Blaabjerg, and Y. Tang, "Highly accurate derivatives for LCL-filtered grid converter with capacitor voltage active damping," *IEEE Trans. Power Electron.*, vol. 31, no. 5, pp. 3612–3625, May 2016.

[52] J. Dannehl, F. W. Fuchs, S. Hansen, and P. B. Thogersen, "Investigation of active damping approaches for PI-based current control of grid-connected pulse width modulation converters with LCL filters," *IEEE Trans. Ind. Appl.*, vol. 46, no. 4, pp. 1509–1517, Jul.–Aug. 2010.

[53] S. G. Parker, B. P. McGrath, and D. G. Holmes, "Regions of active damping control for LCL filters," *IEEE Trans. Ind. Appl.*, vol. 50, no. 1, pp. 424–432, Jan.–Feb. 2014.

[54] J. Samanes, A. Urtasun, E. Gubia, and A. Petri, "Robust multisampled capacitor voltage active damping for grid-connected power converters," *Int. J. Elect. Power Energy Syst.*, vol. 105, pp. 741–752, 2019.

**David Lumbreras** (S'18) was born in Pamplona, Spain, in 1993. He received the B.Sc. and M.Sc. degrees in electrical engineering, in 2015 and 2017, respectively, from the Public University of Navarre, Pamplona, Spain, where he is currently working toward the Ph.D. degree. He did his Master's Thesis at the Technische Universität Braunschweig, Braunschweig, Germany, on the topic of advanced control for power electronics.

In 2015, he joined the Electrical Engineering, Power Electronics and Renewable Energy Research Group, Public University of Navarre. His research interests include power electronics, design of power converters, and renewable energies.

**Ernesto L. Barrios** (S'12–M'16) was born in Pamplona, Spain, in 1988. He received the B.Sc., M.Sc., and Ph.D. degrees in electrical engineering from the Public University of Navarre, Pamplona, Spain, in 2009, 2012, and 2015, respectively.

In 2011, he joined the Electrical Engineering, Power Electronics and Renewable Energy Research Group, Public University of Navarre, where he is currently an Associate Professor and a Researcher. During six months in 2016, he was an Academic Guest with the Power Electronic Systems Laboratory, ETH Zürich, Zürich, Switzerland. His main research interests include high-frequency magnetics, wide bandgap power semiconductor devices, and power converters for renewable energies, particularly for photovoltaics and fuel cells.

**Andoni Urtasun** (S'11–M'16) was born in Pamplona, Spain, in 1987. He received the M.Sc. degrees in electrical engineering from the Public University of Navarre (UPNA), Pamplona, Spain, and the Institute National Polytechnique de Toulouse, Toulouse, France, both in 2010, and the Ph.D. degree in electrical engineering from the UPNA in 2015.

In 2010, he joined the Electrical Engineering, Power Electronics and Renewable Energy Research Group, UPNA, where he is currently an Assistant Professor. During 2014, he was a Visiting Scholar with The University of Sydney, Camperdown, NSW, Australia. His research interests include power electronics and renewable energies.

**Alfredo Ursúa** (M'04) received the B.Sc. (Hons.), M.Sc. (Hons.), and Ph.D. degrees in electrical engineering from the Public University of Navarre, Pamplona, Spain, in 2001, 2004, and 2010, respectively.

In 2002, he joined the Department of Electrical, Electronic and Communications Engineering, Public University of Navarre, where he is currently an Associate Professor. He is currently the Vice Dean of the School of Industrial & ICT Engineering and a member of the Steering Committee of the University Chair for Renewable Energies. He has coauthored more than 60 journal papers and conference contributions, supervised three Ph.D. theses, and holds two patents. He has been involved in several research projects both with private and public funding, and mainly related to renewable energy systems, electric energy storage technologies, power electronics, energy management, and electric microgrids.

Dr. Ursúa is currently a member of the Spanish Hydrogen Association.

**Luis Marroyo** (M'04) received the M.Sc. degree in electrical engineering from the University of Toulouse, Toulouse, France, in 1993 and the Ph.D. degrees in electrical engineering from the Public University of Navarre (UPNA), Pamplona, Spain, in 1997 and from the LEEI-ENSEEIHT INP Toulouse, France, in 1999.

From 1993 to 1998, he was an Assistant Professor with the Department of Electrical and Electronic Engineering, UPNA, where he has been an Associate Professor since 1998. He is currently the Head of the INGEPER Research Group. He has been involved in more than 70 research projects mainly in co-operation with industry, he is the co-inventor of 20 international patents and co-author of more than 100 papers in international journals and conferences. His research interests include power electronics, grid quality, and renewable energy.

**Pablo Sanchis** (M'03–SM'12) received the M.Sc. degree in management and business administration and the M.Sc. and Ph.D. degrees in electrical engineering from the Public University of Navarre (UPNA), Pamplona, Spain, in 1994, 1995, and 2002, respectively.

From 1996 to 1998, he was a Guest Researcher with the Delft University of Technology, Delft, The Netherlands. In 1998, he joined the Department of Electrical, Electronic and Communications Engineering, UPNA, where he is currently an Associate Professor. He is also the Director of the UPNA Chair for Renewable Energies and the Director of the Research Resources and Structures Unit of the university. He was the Vice Dean of the School of Industrial and Telecommunications Engineering. He has been involved in more than 70 research projects both with public funding and in co-operation with industry and is the co-inventor of eight patents. He has also co-authored more than 140 papers and contributions in international journals and conferences, and supervised nine Ph.D. theses. His research interests include renewable energies, power electronics, electric energy storage technologies, grid integration of renewable energies, and electric microgrids.

Dr. Sanchis was the recipient of the UPNA Research Award in 2013 for the Best Technical Paper and the UPNA Excellence in Teaching Award in 2017.